

This material is subject to protection under local, state, federal, and international copyright laws. (Title 17 U. S. Code)

[Menu]

7 Requests(s)

1) RAPID #
-370777



-370777

Done Printing

BORROWER
ORU



128.223.84.143

CALL #: TK9001 .N755
LOCATION: ENGINE

TYPE: Article
USER JOURNAL TITLE: Nuclear Engineering and Design
OCLC JOURNAL TITLE: Nuclear engineering and design
COD CATALOG TITLE: Nuclear engineering and design : an international journal devoted to the thermal, mechanical and structural problems of nuclear energy
ARTICLE TITLE: Sugano, et al "Full Scale Aircraft Impact Test..."
VOLUME: 140
NO:
YEAR: 1993(1993)
PAGES: 373-385
ISSN: 0029-5493
OCLC #: 6033981
VERIFIED: unverified

PATRON: Russell, Gerald S.
PATRON ID: .p1169946
PATRON PHONE:
PATRON DEPT: none
PATRON STATUS: PTYPE:14
PATRON FAX:
PATRON ADDRESS:640 Deertrail Rd Eugene OR 97405
PATRON E-MAIL:
PATRON NOTES: jerry-r@comcast.net;

Full-scale aircraft impact test for evaluation of impact force

T. Sugano ^a, H. Tsubota ^a, Y. Kasai ^a, N. Koshika ^a, S. Orui ^a, W.A. von Rieseemann ^b,
D.C. Bickel ^b and M.B. Parks ^b

^a *Kobori Research Complex, Inc., Tokyo, Japan*

^b *Sandia National Laboratories, Albuquerque, NM, USA*

Received 19 March 1992, revised version 25 December 1992

Previously, estimates of the force caused by aircraft impact into rigid structures have been determined using theoretical methods based on the aircraft's calculated mass and strength distribution. However, these methods required many assumptions to be made and they left many questions unanswered. Because of the uncertainty involved in these analytical predictions of impact force, a full-scale aircraft impact test was performed and an extensive set of response measurements was analyzed to evaluate the impact force against a rigid target. The analysis and evaluation gave an accurate impact force–time curve under the test condition and confirmed the practical use of an existing analytical method. An analysis with a lumped mass spring model also provided good agreement with the test results.

1. Introduction

To estimate the global elasto-plastic structural response of critical concrete structures subjected to an aircraft crash, the time dependent force caused by a normally impacting aircraft against a flat rigid barrier must be known. A significant problem has been the lack of experimentally validated methods to estimate the force caused by aircraft impact against a rigid target.

Many previous researchers, such as Hornyik [1], Riera [2], Drittler and Gruner [3,4], Wolf et al. [5], Rice and Bahar [6], Kar [7] and Riera [8], have derived forcing functions by analysis using the impact velocity of the aircraft and its calculated mass and strength distribution. However, these previous analytical methods required many assumptions to be made and they left many questions unanswered. Because of the uncertainty involved in these analytical predictions of impact force, a full-scale aircraft impact test was performed by Sandia National Laboratories in the U.S.A. and an extensive set of response measurements was obtained.

This paper first describes the test plan, method and results. Next, the measurements are analyzed to determine the impact force. The results were also used to evaluate existing analytical methods for predicting the impact force.

2. Test plan

2.1. Purpose of the test

The primary purpose of the test was to determine the impact force as a function of time for the impact of a F-4 Phantom onto a massive, essentially rigid, reinforced concrete target. An impact velocity of 215 m/s, corresponding to that of the full-scale engine impact tests performed previously [11], was employed for the test. The impact orientation was assumed to be head-on, i.e., normal to the target. Additional objectives of the test were: (a) to determine the crushing behavior of the aircraft, (b) to determine if the engines broke away from the aircraft before their impact, and if so, to measure their impact velocity, and (c) to record the dispersal of 'fuel' after impact (water was used as a surrogate for the fuel).

2.2. Test method

An existing 600-m-long two-rail rocket sled facility located at Sandia National Laboratories in Albuquerque, New Mexico, USA was used to perform the test. This facility has been used in conducting many tests, such as the impact of spent-fuel shipping casks, turbine missiles [13] and turbojet engines [11]. Knowl-

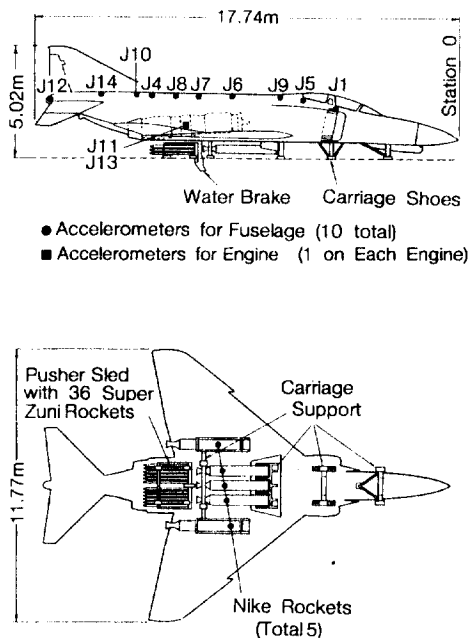


Fig. 1. F-4 Phantom test configuration.

edge gained from many previous tests was utilized in this aircraft test.

Aircraft

A flyable F-4D aircraft, as shown in fig. 1, was acquired by Sandia for the test. This aircraft weighed 12.7 tonnes with some avionics equipment and seats removed. It was modified slightly so that it could be supported on the rocket sled rails at four locations with a special carriage structure. The front gears, main gears and flaps at the main wings were removed, and sleds for the test and rockets for propulsion were attached at these locations. These attachments were designed break away from the fuselage on impact.

The carriage structure had "shoes" that wrapped around the flanges of the rails to prevent lift-off and to guide the aircraft. The impacting weight was 19.0 tonnes, including the weight of the above attachments, five rocket casings and 4.8 tonnes of water which was added to simulate the fuel weight and at the same time to provide the proper mass distribution. The mass distribution for an 'original' F-4D is shown in fig. 2, while the mass distribution of the F-4D as configured for the impact test is shown in fig. 3.

Target

The target consisted of a block of reinforced concrete 7 m square and 3.66 m thick mounted on a platform, as shown in fig. 4. It had a weight of 469

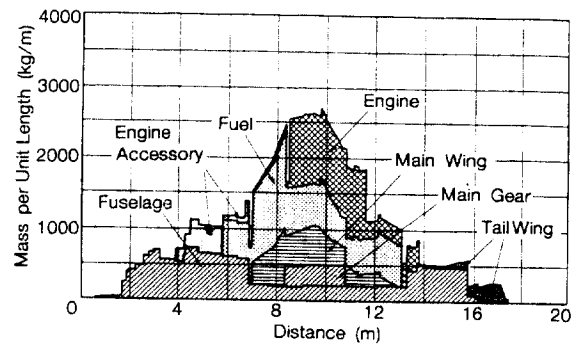


Fig. 2. Mass distribution of an original F-4D.

tonnes (almost 25 times the weight of the F-4D). The target sat on top of a foundation mat slab cast immediately in front of a back-up structure. The platform, in which air-bearings were placed, was 0.56 m thick and was cast on the top of the foundation mat. Because of the difficulty in accurately estimating the friction between two rough, sliding surfaces, the friction between the two surfaces was reduced to an insignificant amount by a unique application of air bearings, which effectively supported the target on a thin layer of air. Ten air bearings were installed in "pockets" in the lower surface of the platform. After inflating the air bearings, a force of only 816 kg (less than 0.2% of the weight of the target) was required to initiate movement of the target. To ensure that the target (concrete block plus platform) would move as a unit, a concrete lip was cast around the upper edges of the platform. The concrete block sat inside this lip.

Propulsion method

To keep the maximum accelerations within the structural limits of the attachment points of the aircraft and of the carriage system, propulsion was provided by a two-stage rocket system. The first stage consisted of a 'pusher' sled housing 36 super Zuni rockets. The pusher

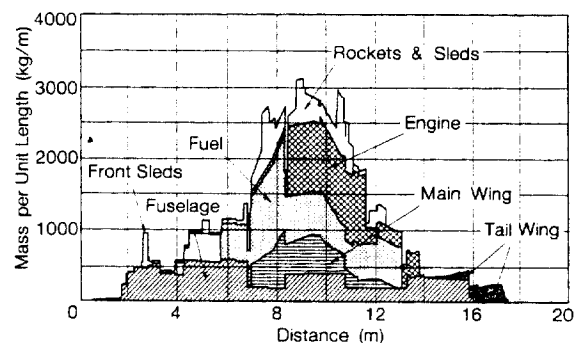


Fig. 3. Mass distribution of F-4D for impact test.

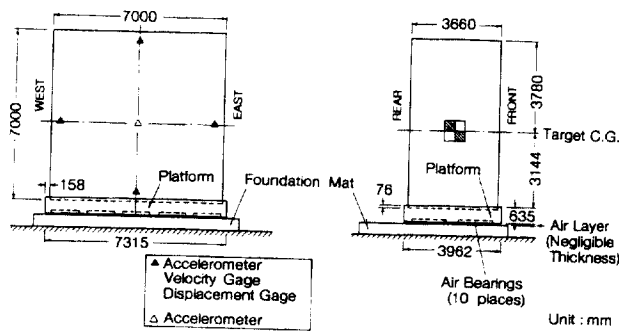


Fig. 4. Target.

sled was stopped by means of a water brake located 70 m for the ignition point. The second acceleration stage was provided by five Nike rockets attached directly to the F-4D.

Measurement

A break-rod system on the track and an image-motion camera were used to measure the velocity of the aircraft just before impact. The break-rods were made of wood with a thin metal strip attached to their surfaces. They were installed at three points near the end of the track, as shown in fig. 5. They were broken by the front shoe of the carriage structure as it passed, thus providing a unique signal to the recording device. The distance between the break-rods divided by the time interval between breaks provided a measurement of aircraft velocity. In addition, images of the aircraft were recorded on film by the image-motion camera as a function of time as the aircraft passed within the camera's field of view. This was also used to determine an estimate of the aircraft velocity at impact.

Ten accelerometers were placed along the top of the aircraft's fuselage (fig. 1) to measure the decelerations as functions of time during the impact sequence. An accelerometer was also attached to the aft flange of each engine. A telemetry package mounted in the tail section of the aircraft was used to transmit the readings.

Two methods, break-wire systems and high speed photography, were used to monitor the possible detachment of the engines from the fuselage before their impact. A total of four break-wire systems, installed between the engines and the fuselage, were used to detect engine detachment. One set of break-wires was fastened to the outboard side at the rear end of each engine and one to the inboard side. Each set of break-wires was wired in a parallel circuit such that a break in a particular wire changed the circuit voltage by a given magnitude.

To determine engine detachment by high-speed photography, the lower rear portions of the engines covers were removed. The exposed parts of the engines and the area of the fuselage just above the exposed portion of each engines were painted red with black vertical stripes.

The details of the impact sequence were recorded by 4 tracking cameras and 16 high-speed framing cameras with frame rates varying from 500 to 2000 frames/second. Photometric targets were painted on the aircraft and the test panel to aid in the reduction of the films. High-speed photography was also used for an overall documentary of the test. Furthermore, physical damage occurring in the test, the dispersion of water and pieces of the crushed aircraft, and the surface damage to the target, were recorded.

Four displacement gages, four velocity gages and five accelerometers were installed on the rear face of the target to measure the motion of the target after impact (fig. 4). One displacement and velocity gage was installed at each edge of the target, with 508 mm of travel. The accelerometers were installed in the same four positions with an additional accelerometer located at the centroid of the target.

2.3. Test results

Physical damage to aircraft and target

The data from the break-rod system and the image-motion camera indicated an impact velocity of 215 m/s ± 1%.

The aircraft impacted the target at a perfectly normal orientation and was crushed from the front of the aircraft as shown in fig. 6. The remainder of the aircraft from the nose to the tail was completely de-

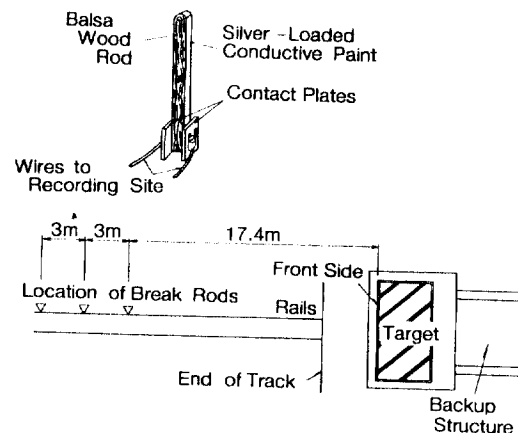


Fig. 5. Break rod.

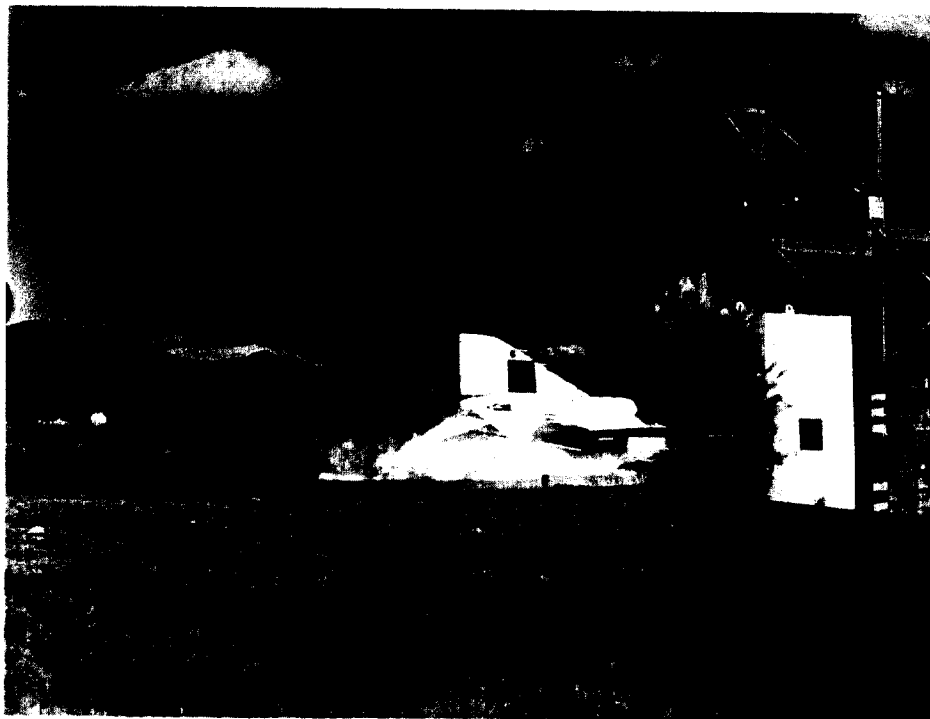
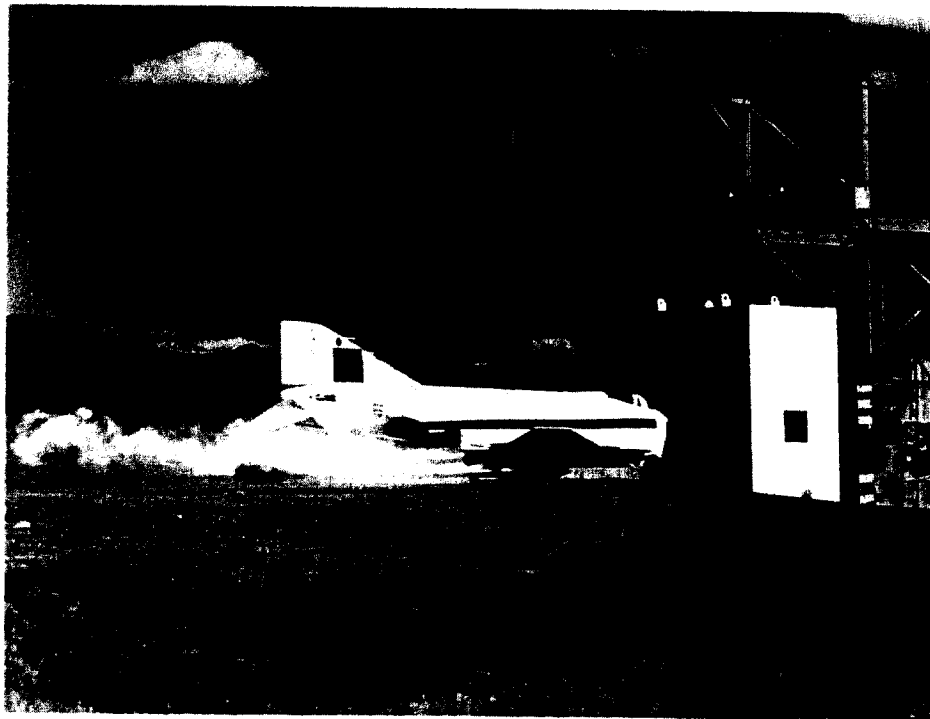


Fig. 6. View of the aircraft during impact.

stroyed during impact. Pieces of the aircraft and lumps of crushed engines were found over a large area concentrated on each side of the target rather than in front of it. The damage to the engines was very similar to that observed in the engine impact tests [11]. The water, that was used instead of fuel, spread to both sides and to the top of the target. Its area was smaller than that of the aircraft.

Damage to the target was relatively minor, as shown in fig. 7, indicating that the major portion of the impact energy was absorbed in moving the target and not in producing structural damage. The face of the target was scarred where the aircraft fuselage struck, but only superficial damage was inflicted over this region. The penetration depth of the engines, which appear as the 'eyes' of the aircraft in the figure, was a maximum of 60 mm, and that caused by the fuselage was a maximum of 20 mm. The load damage caused by the fuselage was insignificant compared with the damage caused by the engines. Most of the damage was done by the carriage structure and the Nike rocket cases. Concrete spalled off the front face of the target from

the level of the rocket case mounts and the carriage structure to the bottom of the vertical panel. The target was displaced 1.83 m against the back-up structure and rebounded. Note that impact of the target into the backup structure occurred after all the data of interest had been obtained.

Target response

Five acceleration measurements are shown in fig. 8. As can be seen, the upper acceleration is slightly larger than the lower acceleration and the two sides (west and east) have almost the same shapes and magnitudes. This indicates that the target experienced a slight rocking motion during impact. To exclude the rocking and other components from the raw acceleration data and obtain an estimate of the horizontal acceleration of rigid motion, these 5 records were averaged. The results are shown in fig. 9. Some typical velocity and displacement measurements are shown in figs. 10 and 11. Also shown are the integration results of the measured accelerations and velocities, which are in excellent agreement with the measured velocities

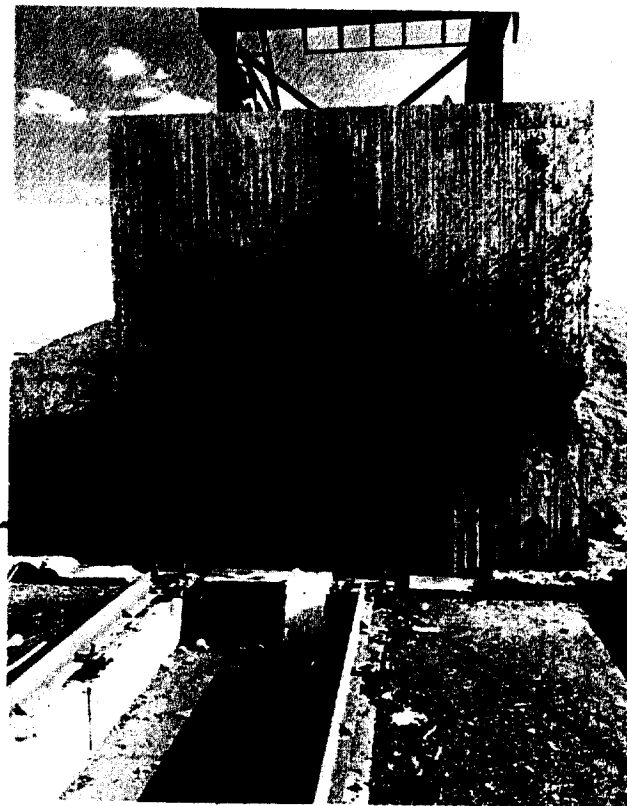


Fig. 7. Target damage.

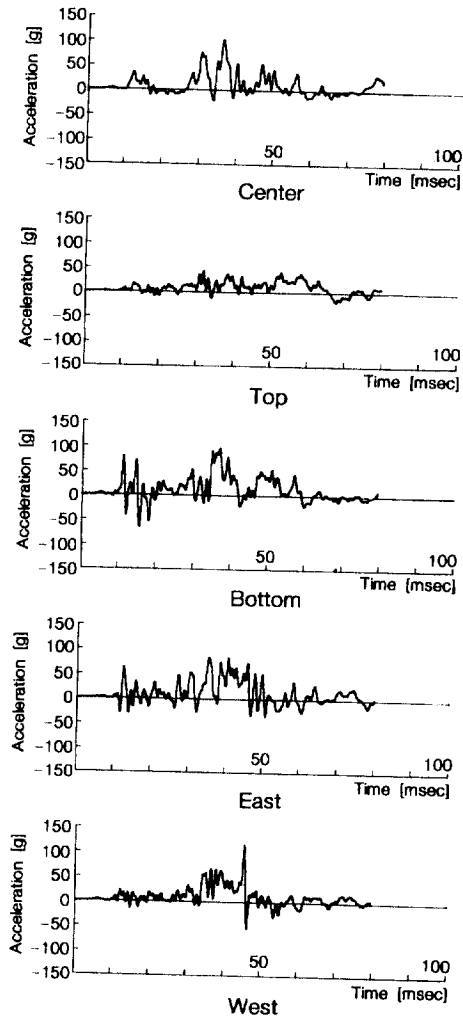


Fig. 8. Five target acceleration measurements.

and displacements, respectively. The major acceleration began about 20 ms after impact and ended about 60 ms after impact. The velocity also began to increase rapidly after 20 ms, indicating that the major force was applied at about that time. The average velocity was

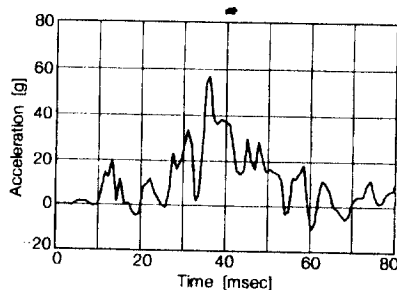


Fig. 9. Average of the five target acceleration measurements.

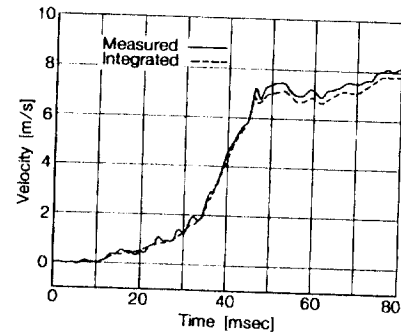


Fig. 10. Measured velocity and time integrated acceleration at west side of target.

nearly constant after 65 ms. This indicates that the impact force was essentially zero after this time and that the target continued to move in free motion until it impacted the back-up structure. It was also confirmed by observation that there was no rubbing scar on the foundation mat caused by the rocking motion.

Aircraft sensor responses

Decelerations of the aircraft was recorded successfully by the accelerometers placed along the top of the fuselage and on both engines. However, the recorded decelerations included noises and pulses transmitted from the crushed portion. These high frequency components were removed by a low-pass filter. Time integration of the filtered deceleration provided the reduction in velocity of the uncrushed portion of the aircraft.

Some typical deceleration measurements, J10(fuselage) and J13(engine), are shown in Figs. 12 and 13. Time integration of these decelerations provided the reduction in velocity versus time from initial impact until the sensors were destroyed. Red vertical stripes were painted on the fuselage at the same axial locations as the accelerometers. This enabled differential crushing of the fuselage to also be examined from the high-speed photography data. Finally, the reduction in

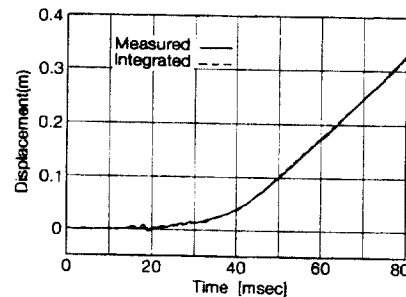


Fig. 11. Measured displacement and time integrated velocity at west side of target.

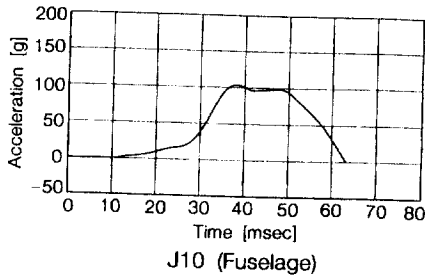


Fig. 12. Measured acceleration at station J10 on the fuselage (filtered).

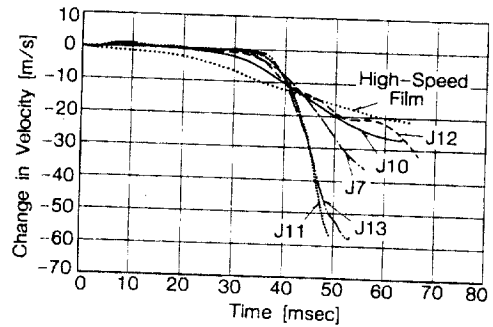


Fig. 14. Velocity reduction curve of aircraft.

velocity is shown in fig. 14. This figure includes other velocity reduction curves at typical points. Reduction curves for the fuselage (J7, J10, and J12) and the data from the high-speed camera show a similar tendency of only slight reduction in velocity. The records for each engine show good agreement and indicate higher velocity reduction than the fuselage.

Detachment of the engines was determined by high-speed photography of the marks painted on the exposed portion of each engine and by the previously described breakwire system. Close-up photographic coverage of this region of the aircraft during impact indicated no relative motion of either engine with respect to the fuselage. The recorded failure times of the break-wires indicated that the engines did not move forward with respect to the fuselage before the impact; however, on impact they were detached.

3. Evaluation of impact force

3.1. Review

One of the first papers on aircraft impact force was written by Riera [2]. He introduced certain assumptions which form the basis of the so-called "Riera approach" for a normal impact on a rigid target. These

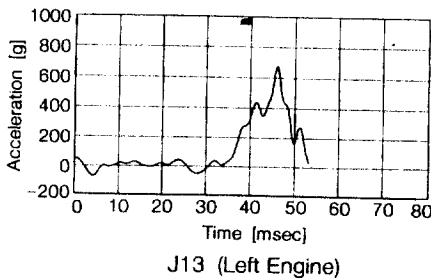


Fig. 13. Measured acceleration at station J13 on the left engine (filtered).

assumptions were that (a) the aircraft is separated into crushed and uncrushed regions and crushing occurs only at the cross-section in contact with the target, (b) buckling of this cross-section decelerates the remaining uncrushed portion which behaves rigidly, and (c) the material behavior of the fuselage is perfectly rigid-plastic. Based on these assumptions, the impact force, F , against a rigid target can be derived at any given time, t , from the momentum equation. The impact force may be expressed as

$$F = P_c + \mu V^2 \tag{1}$$

in which the following parameters are evaluated at time, t , during impact: P_c = load necessary to crush the fuselage at the impact interface, μ = mass per unit length of the uncrushed portion, and V = velocity of uncrushed portion. Based on this approach, Riera evaluated the force-time relationship for a Boeing 707-320 with an assumed distribution of mass and buckling load.

Drittler and Gruner performed a dynamic elasto-plastic analysis and calculated the load-time function of the aircraft engine [3] and the F-4 Phantom [4]. In this analysis, the projectile model is divided into elements along the flight trajectory. Different elastic and plastic material properties for each element can be taken into account. The computation algorithm is based on a difference method.

Hornyik [1] basically made the same assumption as Riera and introduced a coefficient less than unity in the second term of the right side of eq. (1), based on the energy conservation law considering the residual energy of the mass, that is, the deformed mass that moves as incoherent small pieces. Riera [8] evaluated the possible use of a coefficient in the second term by considering the thermal and kinetic energy in the direction normal to the target surface in the energy balance. However, due to a lack of sufficient experi-

mental evidence and difficulty in evaluating the energies, the coefficient could not be derived.

Kar [7] considered that the remaining material piled up at the impacting end of the aircraft and introduced a coefficient α into the second term of the right-hand side of eq. (1). Then,

$$F = P_c + \alpha\mu V^2. \quad (2)$$

Bahar and Rice [6] considered that the velocity distribution in the crushed region of the aircraft decreases to zero at the rigid wall, and derived a coefficient α equal to 0.5.

Wolf et al. [5] checked the validity of Riera's approach of modeling the aircraft as given by eq. (1). He compared the resulting force-time function with that from a more elaborate one-dimensional lumped mass dynamic elasto-plastic model of a Boeing 707 impinging onto a rigid target. This indicated that the two models agree extremely well for all impact velocities in the force-time diagrams. Zorn and Schueller [9] evaluated the load-time curve for normal and oblique impact of a Phantom aircraft using a discrete mass model interconnected by axial and rotational springs.

In the present study, a full-scale aircraft impact test was performed to clarify the unknown coefficient α in eq. (2) experimentally. As described in Section 3.3, this test yielded a value for the coefficient α . It was also confirmed that a simulation analysis using a lumped mass model was a good representation of the behavior of the aircraft and target during impact.

3.2. Method of evaluating impact force from test measurements

In principle, an impact force, F , generated over a time interval dt corresponds to the changing rate of a momentum (MV) during, dt . Therefore,

$$F = \frac{d}{dt} [MV], \quad (3)$$

where V = velocity of mass M . The right-hand side of eq. (3) expresses an inertial force caused by the change in velocity and the force required to decelerate the mass of the impinging cross-section. Eq. (3) can be rewritten as,

$$F = M \frac{dV}{dt} + V \frac{dM}{dt}. \quad (4)$$

In the F-4 test, kinematic measurements were made by sensors mounted on the aircraft and the target test panel. Therefore, the total impact force, F , could be

evaluated independently from the change in momentum of the target and from the aircraft.

The target was essentially rigid. Therefore, little energy went into its structural deformation and there was essentially no change in its mass. The target's mass was about 25 times the aircraft's mass. The friction force was very small (less than 0.2%). Therefore, the second term of eq. (4) is negligible and essentially all the energy went into moving the target. Introducing the measured mass and acceleration of the target into eq. (4), the total impact force on the target, F_t , can be evaluated at any time, t , impact as simply,

$$F_t = M_t a_t \quad (5)$$

in which M_t = mass of the target and a_t represents the target acceleration at the time for which the impact force is being calculated.

The impact forcing function was also determined from the aircraft response. For the aircraft, both terms of eq. (4) are required. They may be evaluated from the response measurements (accelerometers) of the aircraft. Writing,

$$\frac{dM}{dt} = \alpha\mu V. \quad (6)$$

Substituting eq. (5) into eq. (4), the impact force at any given time, t , may be evaluated from the aircraft measurements as:

$$F_a = M_a \frac{dV_a}{dt} + \alpha\mu(V_a - V_t)^2, \quad (7)$$

where F_a = impact force evaluated from measurement of the aircraft, M_a and V_a = mass and velocity, respectively, of the uncrushed portion of aircraft, V_t = target velocity, and α is defined as a coefficient of effective mass on impact.

Engines and sleds were confirmed in the test to be detached from the fuselage when the head of each part touched the target. Thus, the impact forces of each part are evaluated independently and then summed to obtain the total load F_a .

3.3. Impact force

Consequently, as shown in fig. 17, two impact force functions, F_t (target) and F_a (aircraft), are derived from the test measurements. These two functions should be essentially the same if the principle of momentum conservation is applicable, there are no other energy losses and the recorded measurements and assumed mass distribution are correct. Comparing the two functions, F_t can be regarded as more reliable than

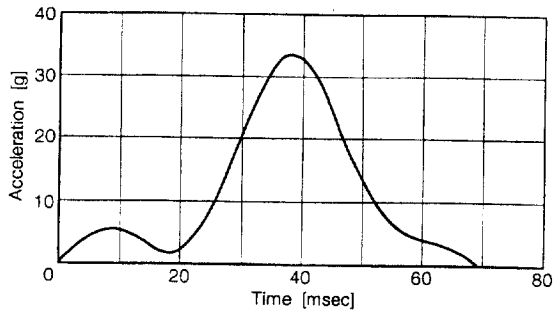


Fig. 15. Acceleration response of target (filtered).

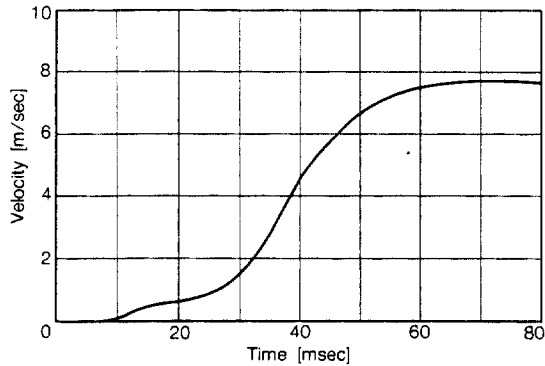


Fig. 16. Velocity response of target (smoothed).

F_a , because F_t is derived directly from accurate measured data, while F_a includes the dispersal of mass at impact, which is not known exactly. This is represented by the factor α . In fig. 17, four functions of F_a are indicated for values of α from 0.7 to 1.0.

To determine a suitable value for α , the impulses are calculated by integrating the impact force functions, and they are compared in fig. 18. The impulse of the target side is obtained by multiplying the target's

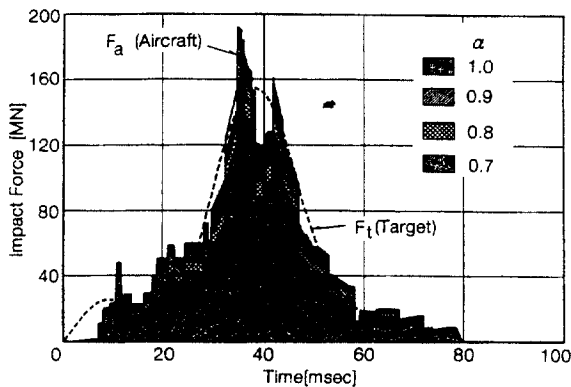


Fig. 17. Impact force (F_t and F_a) versus time curve.

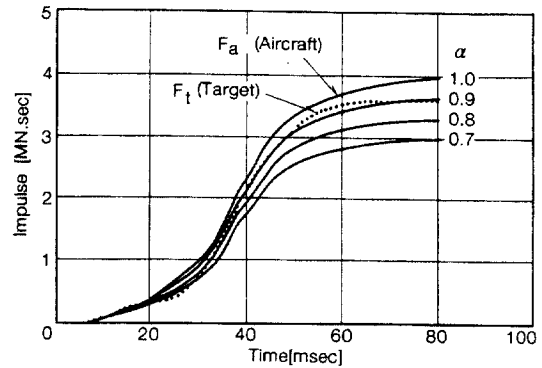


Fig. 18. Impulse of F_t and T_a .

mass by the averaged and smoothed velocity response shown in fig. 16. The total impulse is defined as the impulse at the end of impact force application, and is considered to be the most important value in evaluating the characteristics of the impact phenomena. Therefore, the factor α is determined so that the final impulse of F_a equals to that of F_t . From fig 18, the most suitable value of α can be regarded as approximately 0.9.

The impact force function F_a , using α as 0.9, is shown again in fig. 19, by separating the components.

4. Simulation analysis with lumped mass model

In the perfectly plastic impact model represented by Riera's model [2], the elastic behavior of the projectile is not taken into account. The load is evaluated for each instant of time as the sum of the ultimate plastic force of the cross section and the momentum of the corresponding mass. However, a discrete model in which the lumped masses are interconnected with axial springs can express the elastic behavior of the aircraft and is easy to use for evaluating the interaction between the aircraft and the target during impact. Therefore, a simulation analysis using a lumped mass model was performed to verify the validity of the model for future use.

4.1. Modeling of aircraft

The aircraft used in the test was expressed as a straightforward one-dimensional lumped-mass-spring model. The mass of the aircraft used in the test was lumped in 100 nodes interconnected by axial springs. The axial behavior of the spring was assumed to be of the buckling type, as shown in fig. 20. The target was

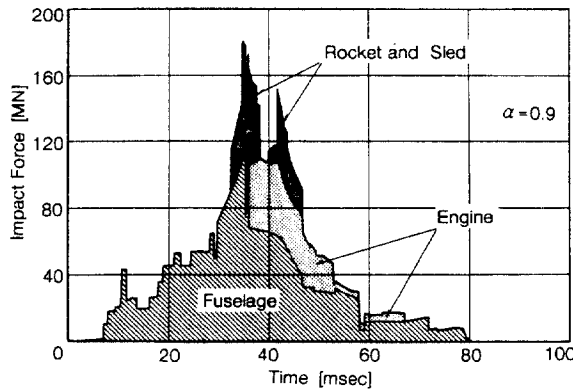


Fig. 19. Impact force of each component (aircraft measurement).

modeled as having one degree of freedom with a very small spring that expresses the friction force between the target and the foundation mat. The analytical model of the target and the aircraft is shown in fig. 20. Based on observations during the test, the engines detached from the fuselage when their heads touched the target and then hit the target independently of the aircraft. Before detachment, the engines and the fuselage behaved as one unit.

4.2. Analytical method

An initial velocity is applied to each node as an initial condition, and the computation algorithm for solving the differential equations is based on the Newmark β method. Nodes of the crushed region of the aircraft are deleted, however, the mass build-up at the target surface is not taken into consideration. Where the strain of the spring connecting two neighboring nodes reaches rupture strain, the masses are assumed to impact ideal-plastically and then form a new node with a combined mass. The velocity of the new node

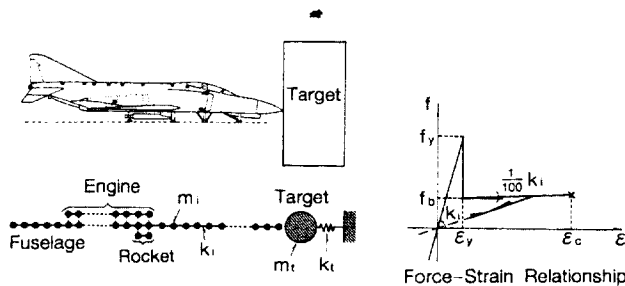


Fig. 20. Aircraft lumped mass model.

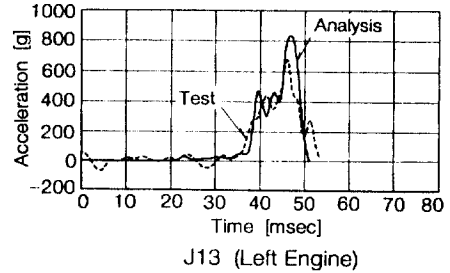
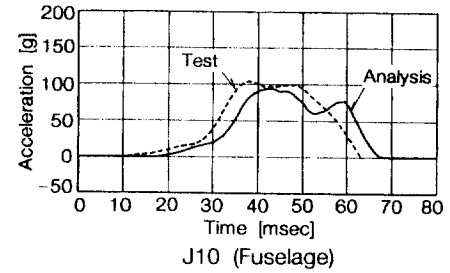


Fig. 21. Analytical results of accelerations at J10 and J13.

just after impact is calculated using conservation of momentum, and the corresponding acceleration is evaluated from the equation of motion at that.

An impact force, F , generated over a time interval, dt , corresponds to the changing rate of momentum, I , during dt . Therefore,

$$F = \Delta I / \Delta t \tag{8}$$

in which, Δt , is the time step. In calculating the impact load, a coefficient of effective mass $\alpha = 0.9$ that is derived from the impact test is used.

Since the change in the aircraft's momentum, I , has a discontinuous state because of the redefined geometry and aircraft mass at each time step, it is necessary to smooth the function, F , to evaluate the load-time function. This can also be performed by applying a moving average of change in momentum for 2-ms time intervals.

4.3. Analytical results

The acceleration responses are shown in fig. 21 and the velocities are shown in fig. 22. High-frequency pulse-like components included in the original acceleration responses have been removed by the smoothing technique used in reduction of the experimental data. These figures show that the analyses agree closely with the test results at the point J10 of the fuselage and the engine.

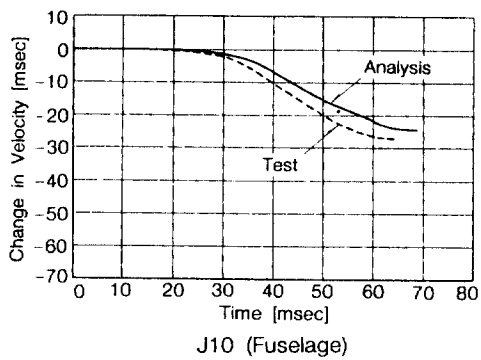
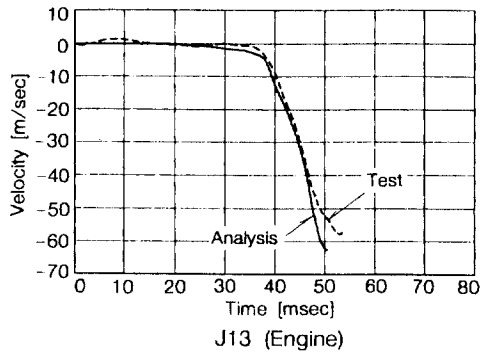


Fig. 22. Velocity reduction curve from analysis.

In fig. 23, the impact load-time function of the analysis is compared with the test result and the values generally show good agreement.

5. Other considerations

5.1. Impact area

To determine the dynamic response analysis of a structure subjected to an impact load, the impact area

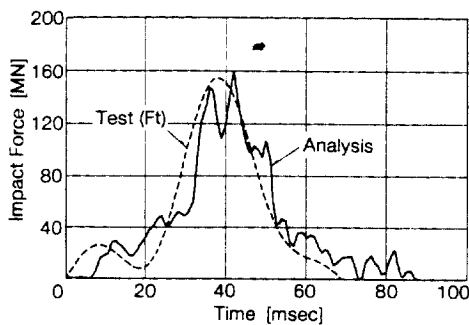


Fig. 23. Impact force versus time curve.

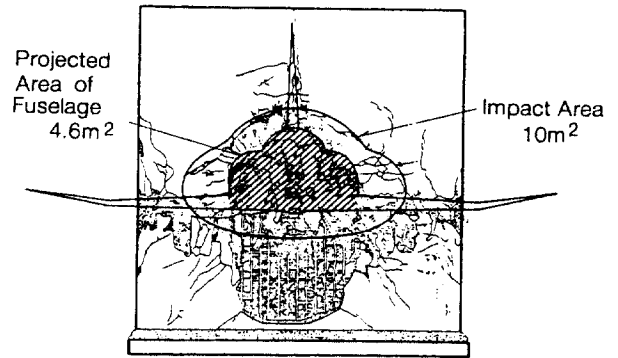


Fig. 24. Impact force area.

must be evaluated. Judging from the damage on the surface of the target, the impact area is about 10 m². This area corresponds to twice the projected area of the fuselage, as shown in fig. 24.

5.2. Aircraft crushing load

Evaluation of crushing load

According to the simple assumption proposed by Riera [2], the crushing load P_c is in equilibrium with the inertial force of the remaining portion of the aircraft. Then,

$$P_c = M_a \frac{dV_a}{dt} \quad (9)$$

To examine the appropriateness of eq. (9), the crippling load of the compressive structural elements of the aircraft was calculated based on the method proposed by Gerard [10]. The measured values of P_c were obtained by evaluating eq. (9) using the data from the F-4 impact test. A comparison between the calculated

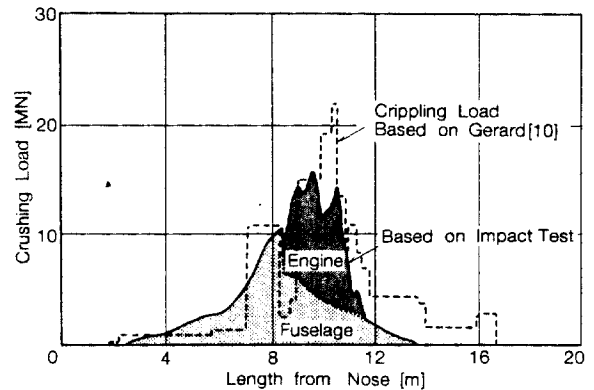


Fig. 25. Crushing load of aircraft.

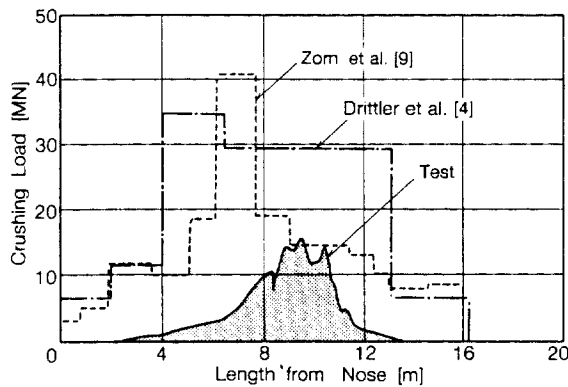


Fig. 26. Comparison of crushing loads.

and measured P_c is shown in fig. 25. The crippling loads prediction method is determined by summing the estimated crippling loads of the various structural elements that make up the fuselage. The dimensions of the elements used to compute of the crippling load of the Phantom were estimated from the skeleton drawing of the fuselage. The figure shows good agreement between the two independent methods.

Crushing load in past study

In past papers, Drittler and Gruner [4] and Zorn and Schueller [9] evaluated the crushing load of an F-4 Phantom using yield strength. The crushing load of the fuselage evaluated from this test is compared in fig. 26 with those given by the other researchers. As shown, the actual fuselage crushing load is about one half of that given in refs. [4,9]. Contrary to the results of previous analyses [4,9], in the test the aircraft was completely crushed to the end of the tail.

5.3. Crushing load component in impact force

The impact force F_a consists of an inertial force corresponding to the crushing load (P_c) described

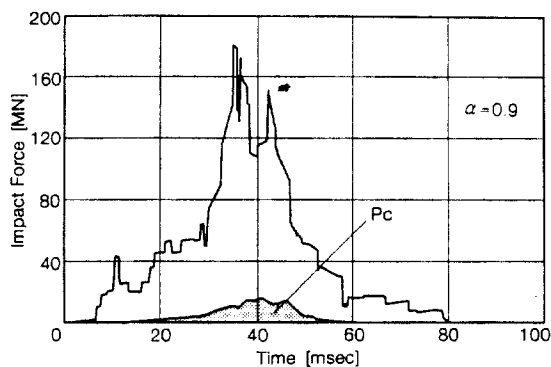


Fig. 27. Crushing load P_c component in total impact force.

above, and a force required to decelerate the mass of the impinging cross-section as shown in eq. (6) and fig. 27. As shown, the crushing load does not greatly affect the magnitude of the impact force. The mass distribution and the coefficient α , which are significant, should be evaluated precisely for evaluation of the impact force.

6. Conclusions

The impact test of a complete F-4 Phantom against a massive, rigid block of concrete floating on a set of air bearings was performed to determine the impact load-time function during aircraft impact. Valuable experimental data obtained from the test was analyzed to evaluate the impact force against a rigid target.

The analysis and evaluation gave an accurate impact force-time curve under the test conditions and confirmed that the existing "Riera approach", with slight modification, is a practical way of evaluating the impact force.

The analysis with a lumped-mass model also represented the test results fairly well.

Acknowledgements

The authors are deeply grateful to the late Dr. Kiyoshi Muto for his great leadership and helpful guidance to this research work.

References

- [1] K. Hornyik, Analytic modeling of the impact of soft missiles on protective walls, Transactions of the 4th International Conference on Structural Mechanics in Reactor Technology, Vol. J 7/3 (1977).
- [2] J.D. Riera, On the stress analysis of structures subjected to aircraft impact forces, Nucl. Engrg. Des. 8 (1968) 415-426.
- [3] K. Drittler and P. Gruner, Calculation of the total force acting upon a rigid wall by projectiles, Nucl. Engrg. Des. 37 (1976) 231-244.
- [4] K. Drittler and P. Gruner, The force resulting from impact of fast-flying military aircraft upon a rigid wall, Nucl. Engrg. Des. 37 (1976) 245-248.
- [5] J.P. Wolf, K.M. Bucher, and P.E. Skrikerud, Response of equipment of aircraft impact, Nucl. Engrg. Des. 47 (1978) 169-193.
- [6] L.Y. Bahar and J.S. Rice, Simplified derivation of the reaction-time history in aircraft impact on a nuclear power plant, Nucl. Engrg. Des. 49 (1978) 263-268.

- [7] A.K. Kar, Impactive effects of tornado missiles and aircraft, *J. of the Struct. Div. ASCE*, Vol. 105, No. ST11 (Nov. 1979) 2243–2260.
- [8] J.D. Riera, A critical reappraisal of nuclear power plant safety against accidental aircraft impact, *Nucl. Engrg. Des.* 57 (1980) 193–206.
- [9] N.F. Zorn and G.I. Schueller, On the failure probability of the containment under accidental aircraft impact, *Nucl. Engrg. Des.* 91 (1986) 277–286.
- [10] G. Gerard, The crippling strength of compression elements, *J. of Aeronaut. Sci.* (Jan. 1958) 37–52.
- [11] K. Muto et al., Experimental studies on local damage of reinforced concrete structure by the impact of deformable missiles Part 3: Full-scale tests, *Trans. 10th International Conference on Structural Mechanics in Reactor Technology*, Vol. J (1989) 271–278.
- [12] K. Muto et al., Full-scale aircraft impact test for evaluation of impact forces, *Trans. 10th International Conference on Structural Mechanics in Reactor Technology*, Vol. J (1989) 285–299.
- [13] R.L. Woodfin, Full-scale turbine missile concrete impact tests, EPRI NP-2745, Sandia National Laboratories (1983).

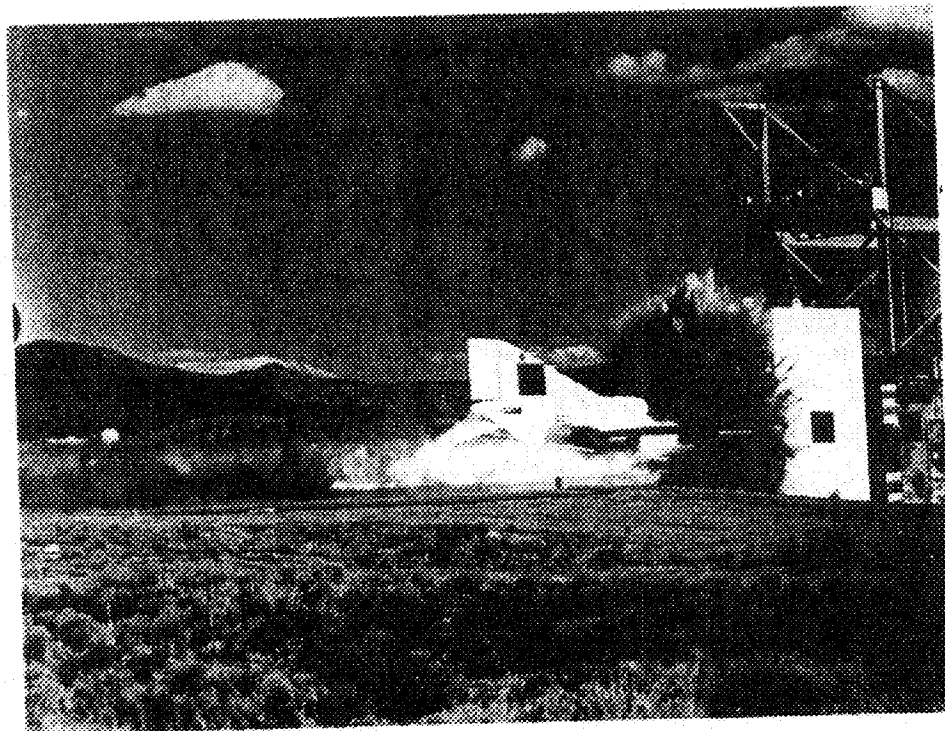
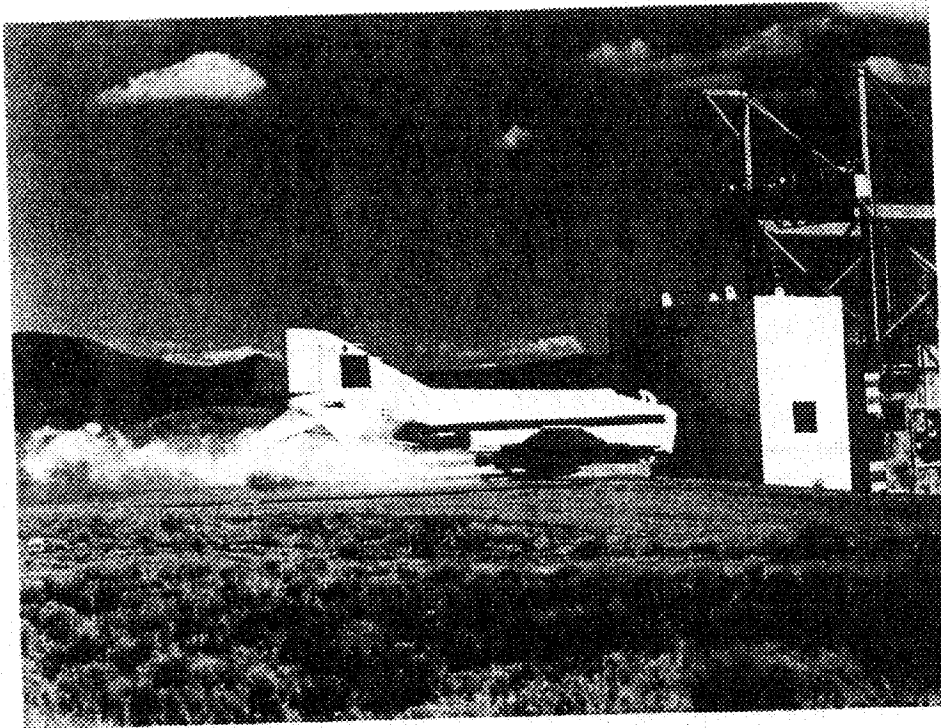


Fig. 6. View of the aircraft during impact.

stroyed during impact. Pieces of the aircraft and lumps of crushed engines were found over a large area concentrated on each side of the target rather than in front of it. The damage to the engines was very similar to that observed in the engine impact tests [11]. The water, that was used instead of fuel, spread to both sides and to the top of the target. Its area was smaller than that of the aircraft.

Damage to the target was relatively minor, as shown in fig. 7, indicating that the major portion of the impact energy was absorbed in moving the target and not in producing structural damage. The face of the target was scarred where the aircraft fuselage struck, but only superficial damage was inflicted over this region. The penetration depth of the engines, which appear as the 'eyes' of the aircraft in the figure, was a maximum of 60 mm, and that caused by the fuselage was a maximum of 20 mm. The load damage caused by the fuselage was insignificant compared with the damage caused by the engines. Most of the damage was done by the carriage structure and the Nike rocket cases. Concrete spalled off the front face of the target from

the level of the rocket case mounts and the carriage structure to the bottom of the vertical panel. The target was displaced 1.83 m against the back-up structure and rebounded. Note that impact of the target into the backup structure occurred after all the data of interest had been obtained.

Target response

Five acceleration measurements are shown in fig. 8. As can be seen, the upper acceleration is slightly larger than the lower acceleration and the two sides (west and east) have almost the same shapes and magnitudes. This indicates that the target experienced a slight rocking motion during impact. To exclude the rocking and other components from the raw acceleration data and obtain an estimate of the horizontal acceleration of rigid motion, these 5 records were averaged. The results are shown in fig. 9. Some typical velocity and displacement measurements are shown in figs. 10 and 11. Also shown are the integration results of the measured accelerations and velocities, which are in excellent agreement with the measured velocities

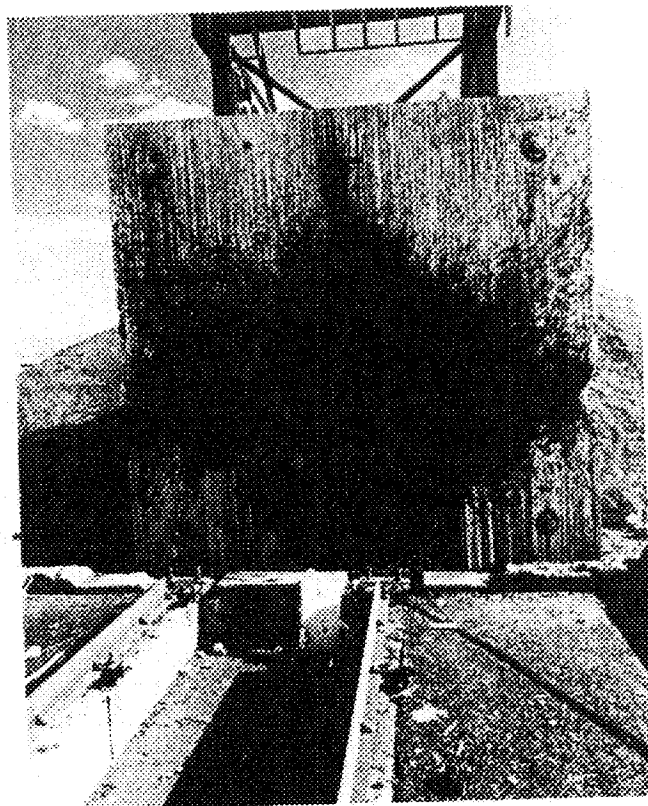


Fig. 7. Target damage.